Quantum Electronics **44** (11) 1022–1028 (2014)

LIGHT SCATTERING

PACS numbers: 42.25.Fx; 61.20.Qg
DOI: 10.1070/QE2014v044n11ABEH015462

Study of the nanobubble phase of aqueous NaCl solutions by dynamic light scattering

N.F. Bunkin, A.V. Shkirin, I.S. Burkhanov, L.L. Chaikov, A.K. Lomkova

Abstract. **Aqueous NaCl solutions with different concentrations have been investigated by dynamic scattering of laser radiation. It is experimentally shown that these solutions contain scattering particles with a wide size distribution in a range of ~10–100 nm. The experimental results indirectly confirm the existence of quasi-stable gas nanobubbles in the bulk of aqueous ionic solutions.**

Keywords: *dynamic light scattering, photon correlation spectroscopy, gas nanobubbles, aqueous electrolyte solutions.*

1. Introduction

Various media, including aqueous electrolyte solutions, which were considered as homogeneous until recently, turned out to be heterogeneous (containing nanoscale inhomogeneities). These inhomogeneities include, first, unremovable solid impurities and, second, gas particles. Specifically the second-type inhomogeneities are of particular interest, because they manifest themselves, for example, in cavitation [1] (one of the causes of erosion and destruction of hydrodynamic systems).

A problem arising in interpreting cavitation phenomena is as follows. The molecular strength of a liquid (tensile pressure under which the latter breaks) is estimated as $\sigma\rho^{1/3}$, where σ is the surface tension coefficient and ρ is the number density of liquid molecules ($\sim 10^4$ atm for water). At the same time, experimental data show that cavitation in water purified of solid impurities may be observed even at a sound wave amplitude of ~1 atm. Thus, cavitation can be excited only when a liquid, free of solid impurity but saturated with dissolved gas (for example, atmospheric air), contains gas bubbles. A theoretical model was proposed in [2] to describe the nucleation and stabilisation of gas nanobubbles in equilibrium ionic solutions under normal conditions (i.e., at room temperature and atmospheric pressure).

A hypothesis about the existence of nanosized bubbles stabilised by ions (bubstons) in these liquids has been put forth. The theoretical model of bubstons was completely developed in [3]. In particular, it was shown that individual bubstons are nanobubbles a few tens of nanometers in size; their size increases with increasing ion concentration in a solution: the bubston radius for aqueous NaCl solutions was found to be 14 and 97 nm at solution concentrations of 10^{-6} and 10^{-2} mol L^{-1}, respectively. In addition, the mechanism of bubston cluster formation was described in [3]; the radius of clusters and their concentration were estimated as functions of the dissolved-ion content.

The situation with cavitation resembles in many respects the situation with the optical breakdown in water [4]: the breakdown threshold for thoroughly purified water is much lower than the ionisation threshold of molecules in water bulk, and the stochastic and multiple character of experimentally observed breakdown indicates the existence of breakdown centres. The optical breakdown model developed in [4] is based on the following hypothesis: the optical-breakdown centres in water and aqueous ionic solutions are also bubstons and bubston clusters, and the breakdown occurs when the focal region of laser beam in a liquid irradiated by laser pulse contains clusters. Experimental data on optical breakdown, interpreted within the bubston-cluster model, were reported in [4, 5].

Along with the studies on optical breakdown, we experimentally investigated bubstons and bubston clusters using phase microscopy [6, 7] and by measuring the angular dependences of the light scattering matrix [8, 9]. Phase microscopy revealed the presence of micrometer-sized particles in aqueous solutions of salts; the refractive index of these particles was smaller than that of water but exceeded the gas-phase refractive index. These particles were interpreted as bubston clusters.

Here, our purpose was as follows: in view of the estimates reported in theoretical study [3], to prove the presence of scatterers with a radius on the order of several hundreds of nanometres, characterise the dependence of their average radius on the NaCl concentration, and prove the influence of the gas content on the formation of these scatterers. NaCl was chosen for the following reason: according to [10], Cl^- anions are adsorbed on the water surface; i.e., these anions can stabilise bubstons, in correspondence with the bubston stabilisation model [2, 3].

N.F. Bunkin A.M. Prokhorov General Physics Institute, Russian Academy of Sciences, ul. Vavilova 38, 119991 Moscow, Russia; N.E. Bauman State Technical University, 2-ya Baumanskaya ul. 5, 105005 Moscow, Russia; Institute of Cell Biophysics, Russian Academy of Sciences, ul. Institutskaya 3, 142290 Pushchino, Moscow region, Russia; e-mail: nbunkin@kapella.gpi.ru;
A.V. Shkirin A.M. Prokhorov General Physics Institute, Russian Academy of Sciences, ul. Vavilova 38, 119991 Moscow, Russia; National Research Nuclear University 'MEPhI', Kashirskoe shosse 31, 115409 Moscow, Russia; e-mail: AVShkirin@mephi.ru;
I.S. Burkhanov P.N. Lebedev Physics Institute, Russian Academy of Sciences, Leninskii prosp. 53, 119991 Moscow, Russia;
L.L. Chaikov P.N. Lebedev Physics Institute, Russian Academy of Sciences, Leninskii prosp. 53, 119991 Moscow, Russia; National Research Nuclear University 'MEPhI', Kashirskoe shosse 31, 115409 Moscow, Russia; e-mail: chaik@sci.lebedev.ru;
A.K. Lomkova N.E. Bauman State Technical University, 2-ya Baumanskaya ul. 5, 105005 Moscow, Russia

Received 6 March 2014; revision received 4 August 2014
Kvantovaya Elektronika **44** (11) 1022–1028 (2014)
Translated by Yu.P. Sin'kov

As follows from the aforesaid, the detection and determination of the parameters of inhomogeneities related to bubstons and bubston clusters is a problem of fundamental importance. Practically, the only method for determining the effective size of nanobubbles in liquid bulk is dynamic light scattering (DLS) (see, for example, [11, 12]). Below we briefly describe the theoretical fundamentals of DLS.

2. Dynamic light scattering

DLS makes it possible to find the diffusion coefficient of dispersed particles in a liquid by measuring the correlation time of scattered-light intensity fluctuations. The nanoparticle radius is calculated from the Stokes–Einstein formula [13] for the diffusion coefficient. Let us consider the diffusion of monodisperse nanoparticles suspended in a liquid. The random Brownian motion of these particles causes fluctuations of their local concentration. In turn, these fluctuations give rise to local inhomogeneities of the refractive index of the medium. When a laser beam passes through this medium, the light is partially scattered from the inhomogeneities, i.e., scattered-light intensity fluctuations are due to the fluctuations of the local concentration of dispersed particles. The light from scattering volume is directed to the photocathode of a quadratic (with respect to the field strength) detector. Beatings between different frequency components of scattered-light spectrum arise on the cathode. Under these conditions, the photocathode illuminance and, correspondingly, photocurrent are amplitude-modulated in a frequency range from zero to some maximum frequency, equal to the full width of the spectral line of Lorentzian profile corresponding to a random diffusion process.

The information about the diffusion coefficient of particles is contained in the time-dependent autocorrelation function of scattering intensity. This function has the form

$$G^{(2)}(\tau) = \langle I(t)I(t+\tau)\rangle = \lim_{t_m\to\infty}\frac{1}{t_m}\int_0^{t_m} I(t)I(t+\tau)\,\mathrm{d}t, \qquad (1)$$

where t_m is the correlation-function accumulation time. Obviously, at $\tau = 0$, the autocorrelation function is equal to the mean-square intensity $\langle I^2\rangle$. At large τ values, there is no correlation, and the autocorrelation function is equal to the squared mean scattering intensity:

$$G^{(2)}(\infty) = \langle I\rangle^2. \qquad (2)$$

In accordance with the Onsager hypothesis [14], the relaxation of concentration fluctuations can be described by the diffusion equation

$$\frac{\partial C(\boldsymbol{r},t)}{\partial t} = -D\Delta C(\boldsymbol{r},t), \qquad (3)$$

where $C(\boldsymbol{r},t)$ is the concentration of particles and D is their diffusion coefficient.

If a system under consideration is characterised by a single diffusion coefficient (for example, a suspension of monodisperse particles in a liquid), the spectrum of the relaxation process and the scattered-light spectral density $S(\omega)$ are described by a Lorentzian (see, for example, [15]). As follows from the Wiener–Khintchin theorem (see, e.g., [16, 17]), this spectrum is related to the autocorrelation function of the scattered-light field E,

$$G^{(1)}(\tau) \equiv \langle E(\tau)E^*(0)\rangle \qquad (4)$$

via the Fourier transform

$$S(\omega) = \int_{-\infty}^{\infty} G^{(1)}(\tau)\exp(-\mathrm{i}\omega\tau)\,\mathrm{d}\tau. \qquad (5)$$

In turn, the normalised intensity correlation function $g^{(2)}(\tau)$ is related to the normalised autocorrelation function $g^{(1)}(\tau)$ of the scattered-light field through the Siegert relation [18]

$$g^{(2)}(\tau) = 1 + f|g^{(1)}(\tau)|^2, \qquad (6)$$

where

$$g^{(1)}(\tau) = \frac{G^{(1)}(\tau)}{G^{(1)}(0)} = \frac{G^{(1)}(\tau)}{\langle E^2\rangle} = \frac{G^{(1)}(\tau)}{\langle I\rangle};$$
$$g^{(2)}(\tau) = \frac{G^{(2)}(\tau)}{G^{(2)}(\infty)} = \frac{\langle I(\tau)I(0)\rangle}{\langle I\rangle^2}; \qquad (7)$$

and f is a dimensionless factor, which takes into account the spatial coherence of scattered light and is determined by the optical installation design.

The autocorrelation function of the light intensity scattered by an ensemble of monodisperse particles suspended in a liquid is described by a decaying exponential in the form [11, 12]

$$G^{(2)}(\tau) = A\exp\left(-\frac{2|\tau|}{t_c}\right) + B, \qquad (8)$$

where $B = \langle I\rangle^2$ [cf. formula (2)] is the 'baseline', determined in experiment by approximating the accumulated function $G^{(2)}(\tau)$ at $\tau\to\infty$, according to expression (8); A is a size constant. In accordance with the solution to diffusion equation (3), the inverse correlation time is [11, 12, 18]

$$1/t_c = Dq^2. \qquad (9)$$

The scattering wave vector $\boldsymbol{q}$ is related (through the Bragg condition) to the spatial Fourier component of fluctuations, which is responsible for scattering at the angle chosen in the experiment. The modulus of this vector, equal to the modulus of the difference in the wave vectors of the scattered and incident waves, is described by the expression

$$q = \left(\frac{4\pi n}{\lambda}\right)\sin\left(\frac{\theta}{2}\right); \qquad (10)$$

this wave number is related to the wavelength of the corresponding Fourier component:

$$\Lambda = \frac{2\pi}{q} = \frac{\lambda}{2n\sin(\theta/2)}. \qquad (11)$$

Here, n is the refractive index of the liquid containing suspended particles and θ is the scattering angle.

There are two methods for measuring the correlation coefficient $g^{(1)}(\tau)$ and, therefore, the and spectral density $S(\omega)$. The first method implies optical heterodyning [19], at which the correlation function of beatings between scattered light and reference laser beam [i.e., directly $g^{(1)}(\tau)$] is measured. The second method is self-beating spectroscopy [17], in which beatings of different frequency components of the scattered-

light spectrum are formed on the cathode. We applied the second method, i.e., measured the normalised intensity correlation function $g^{(2)}(\tau)$ rather than $g^{(1)}(\tau)$.

As was noted above, spherical solid particles with a radius R, subjected to the Stokes friction force $F = 6\pi\eta Rv$ (η is the dynamic viscosity of the medium through which particles of radius R move with a velocity v) can be described by the Stokes–Einstein formula

$$D = \frac{k_B T}{6\pi\eta R}, \tag{12}$$

where k_B is the Boltzmann constant and T is the absolute temperature. For complex-shape particles, R is the average hydrodynamic radius. If we deal with a gas bubble in a liquid, the Stokes friction force is $F = 4\pi\eta Rv$ (see p. 100 in [20]); therefore, to estimate the bubble radius, one must use the formula

$$D = \frac{k_B T}{4\pi\eta R}. \tag{13}$$

Thus, the normalised field correlation function for a suspension of monodisperse particles has the form [15]

$$g^{(1)}(\tau) = \exp(-Dq^2|\tau|) = \exp(-\Gamma|\tau|) = \exp(-|\tau|/t_c), \tag{14}$$

where $\Gamma = 1/t_c$. The spectral density $S(\omega)$ for polydisperse systems consists of several (determined by the number of fractions of particles with different sizes) superimposed Lorentzians, with a common centre at $\omega = 0$. The normalised field-strength correlation function $g^{(1)}(\tau)$ can be presented as a sum of decaying exponentials:

$$g^{(1)}(\tau) = \sum_i A_i \exp\left(-\frac{|\tau|}{t_{ci}}\right), \tag{15}$$

each characterised by a correlation time $t_{ci} = 1/(D_i q^2)$. In this case, the correlation function $G^{(1)}(\tau)$ is analysed by either the histogram method (which is preferred for distributions with several peaks) or by the method of moments. The latter is generally applied for monomodal particle size distributions. Its essence is as follows.

The time dependence of the logarithm of correlation function for a monodisperse sample is linear (see formula (14)), whereas the contribution of nonlinear terms is considerable for polydisperse samples. In this case, one should apply expansion in series in powers of τ:

$$\ln g^{(1)}(\tau) = -\Gamma\tau + C_2\tau^2 + C_3\tau^3 + \ldots. \tag{16}$$

Coefficient Γ in the first term allows one to calculate the mean effective particle radius from formula (12) or (13), the second coefficient C_2 yields information about the width of particles size distribution, and the third coefficient C_3 characterises the distribution asymmetry.

For a polydisperse sample (a case of polymodal distribution, where a suspension contains particles of several characteristic sizes), the method of moments cannot yield information about several peaks in the particle-size distribution. In this case, programs based on the decomposition of the experimentally obtained correlation function $g^{(1)}(\tau)$ in exponentials are applied. Generally speaking, this problem is mathematically ill-posed, and small distortions of this function, caused, for example, by noise or baseline shift (see expressions (2) and (8)) due to the presence of dust, may distort the desired distributions. However, histogram-based constrained regularisation decomposition algorithms [21], for example, CONTIN [22–24] or Dyna [25], have been developed and widely applied. They provide rather adequate decompositions. We applied the DynaLS software [with allowance for formula (13)], which is used by many manufacturers of DLS equipment, such as Edinburgh Instruments (Great Britain), Wyatt Technology Corporation (the United States–EU–China), Becker & Hickl GmbH (Germany), Biosense Webster (the United States), and Photocor Instruments (Russia–the United States). This software was verified by its developers [25] and the aforementioned manufacturers.

2.1. Experimental

We investigated aqueous NaCl solutions with concentrations $10^{-6} < C < 1$ mol L^{-1}, purified from solid impurities and saturated with dissolved gas (atmospheric air), by DLS. Samples were prepared using chemically pure NaCl (with a NaCl fraction of more than 99 wt %) and distilled water with a resistivity 5 MΩ cm and pH = 5.7. Liquid samples were purified from trace solid impurities using a Teflon membrane filter with a pore radius of 100 nm.

The correlation function was measured by the experimental setup, which is schematically shown in Fig. 1. This setup was described in more detail in [26]. Alignment was performed so as to make the cell axis coincide with the goniometer axis and the common axis intersect a focused laser beam. The scattering volume is determined by the boundaries of the laser beam caustic and the field of view of photoelectron multiplier (PEM), i.e., by the image of the diaphragm D formed by objective O. The aperture diaphragm AD provides spatial coherence of scattered light.

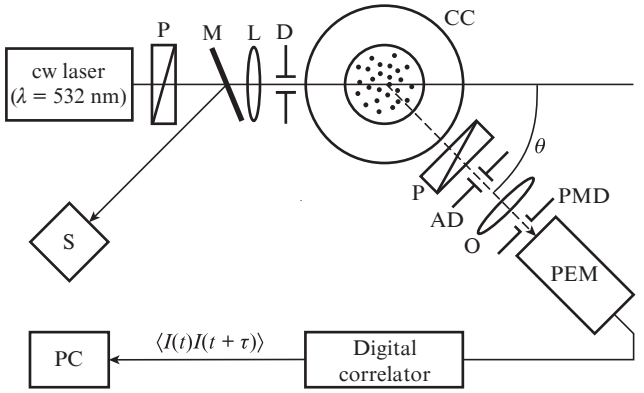

Figure 1. Schematic of the experimental setup for photon correlation spectroscopy: (P) polarisers; (M) 10% mirror; (L) focusing lens; (O) objective; (CC) cylindrical cell with a liquid sample containing scattering particles; (D) diaphragm; (AD) aperture diaphragm; (PMD) photoelectron multiplier diaphragm; (S) incident light intensity sensor.

The measured correlation function was decomposed in a sum of exponentials using the DynaLS software [25], which applies histogram regularisation. One must take into account that this decomposition provides a distribution of scattered-light intensity I over relaxation times t_{ci} [see formula (15)]. Then these times are recalculated into particle sizes using formulas (12) or (13). The particle size distribution can be

obtained if the light-scattering indicatrix function is known. In addition, formulas (8)–(15) can be considered as adequate; therefore, the DynaLS software yields correct results when the scattered light obeys the Gaussian statistics. For a particle suspension, this means that the scattering volume should contain no less than 30 scatterers. Note that the correctness of the distributions obtained can be affected by such factors as double and multiple scattering, presence of dust in the sample, instability of laser power or beam mode structure, etc. Therefore, the applicability of the algorithm for decomposing correlation functions implemented in the DynaLS software was verified for our experimental conditions on calibration suspensions of polystyrene latex particles in distilled water. It was found that, at a size ratio of more than 4:1 for spherical particles from two groups, the size distribution modes can be reliably separated and the radii of polydisperse suspension particles are determined adequately. Figure 2 shows an example of histogram of size intensity distribution, obtained from the correlation function of light scattered at an angle $\theta = 60°$ by a suspension of a mixture of calibrated latex particles with radii of 100 and 480 nm. The volume concentrations of polystyrene particles with these radii, C_{100} and C_{480}, were identical and equal to 1.6×10^{-6}. The processing using the DynaLS software yielded group-average values of 97.4 and 483.4 nm (the distribution peaks are located at 98.9 and 484.5 nm); the ratio of scattering intensity from particles of these two groups is adequately described by the Rayleigh–Gans–Debye approximation [27, 28]. Thus, we can state that our setup was calibrated sufficiently well.

When the number of particles in the scattering volume is small, their statistics ceases to be Gaussian. In this situation, scattered-light intensity fluctuations are due to not only the Brownian diffusion of particles (recall that in the case of monodispersity one deals with a single correlation time: $t_c = 1/(Dq^2)$, whereas in the case of case polydispersity a set of times $t_{ci} = 1/(D_i q^2)$ must be considered) but also a slower process, determined by passage of scattering particles through the laser-beam region or through the PEM field of view. The correlation time of this process is $t_e \sim a^2/D$, where a is the minimum value out of two quantities: the laser-beam radius and the radius of the PEM field of view. Correspondingly, the ratio $t_e/t_c = a^2/\Lambda^2$. For example, at a radius of the PEM field of view $a = 90$ μm, scattering angle $\theta = 45°$, and $\lambda = 532$ nm, we have $t_e/t_c = 1.8 \times 10^4$. In this case, a peak arises in the distribution of scattering intensity I over correlation times; it lies in the range of times significantly exceeding the correlation time due to the Brownian diffusion. The recalculation to particle size R according to formulas (12) or (13) yields two different ranges of scatterer sizes: scatterer radii from 100 nm to 1 μm and radii exceeding 10^5–10^6 nm. Physically, there are no scatterers belonging to the second range; therefore, when estimating the concentrations of particles of different sizes, this range of radii should be simply ignored.

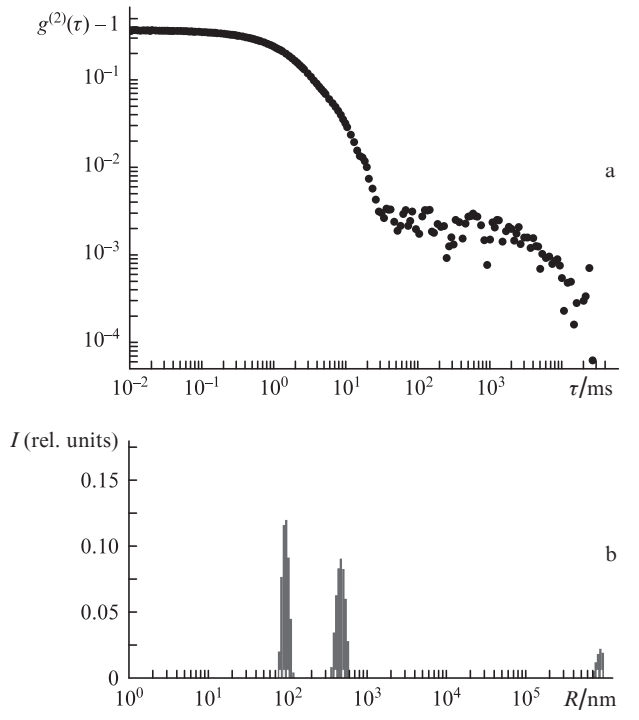

Figure 2. (a) Time correlation function of light intensity scattered at an angle $\theta = 60°$ for a suspension with a mixture of 100- and 480-nm latex particles at $C_{100} = C_{480} = 1.6 \times 10^{-6}$ and (b) the corresponding histogram of scattered-light intensity over effective particle sizes R.

2.2. Experimental results

Below we present experimental data on an aqueous NaCl solution with a concentration of 1 mol L^{-1}. Figure 3 shows function $g^{(2)}(\tau) - 1$ [see formulas (6)–(8)], measured at scattering angles $\theta = 45°$ and 120°.

The processing of this function with the DynaLS software yields intensity histograms of scattered-light intensity distri-

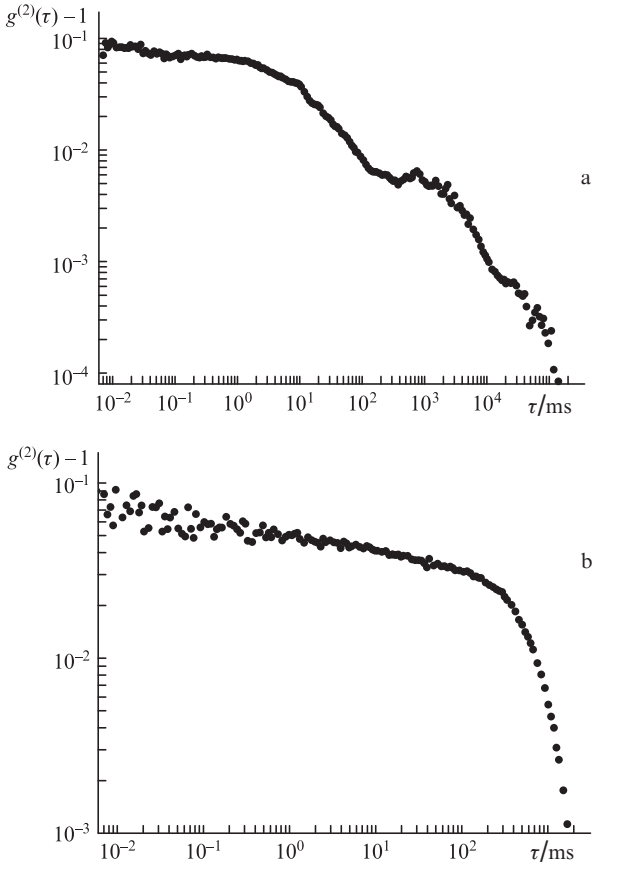

Figure 3. Function $g^{(2)}(\tau) - 1$ for aqueous solution of sodium chloride with a concentration 1 mol L^{-1} for scattering at angles θ = (a) 45° and (b) 120°.

butions over particle sizes; they are shown in Fig. 4. It can be seen that the liquid sample contains particles with radii in the range of $70 < R < 4000$ nm. Note again that the scattering-intensity distribution over scatterer sizes is not identical to the size distribution of scatterers, because the dependence of the scattering cross section on the particle size must be taken into account. Figure 4 exhibits also a mode corresponding to scatterers with a radius of ~1 nm; this mode is due to the total contribution of molecular scattering and photomultiplier autocorrelations. In addition, there is a mode corresponding to scatterers with radii in the range of $\sim 10^5 - 10^6$ nm. In our opinion, this mode is due to the passage of particles through the region corresponding to the PEM field of view (see above).

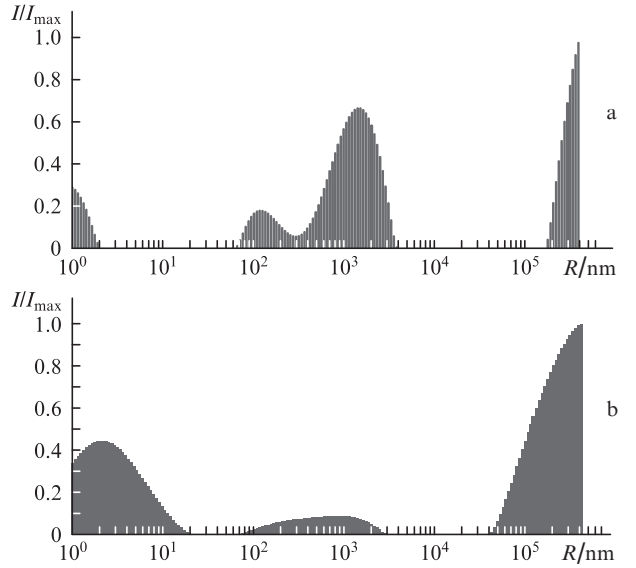

Figure 4. Light-intensity distribution histograms [scattering at angles θ = (a) 45° and (b) 120°] over particle sizes in a sample of aqueous NaCl solution with a concentration of 1 mol L^{-1}.

Having compared the scattering intensity in NaCl solutions with a concentration of 1 mol/l and in toluene, whose scattering coefficient is known (see, for example, [29]), we could estimate the bubston concentration n_b in these solutions. Since the refractive index of the largest bubston aggregates is about 1.28 (according to the phase microscopy data [8]), the ratio $\Delta n/n_{H_2O} \approx 0.04$, and a rough estimation can be performed within the Rayleigh–Gans–Debye approximation [27, 28]; this estimation yields $n_b \sim 10^5 - 10^7$ cm^{-3}. The number of particles in a scattering volume of 5×10^{-5} cm^3 is ~5–500; i.e., the condition of Gaussian statistics for scattering intensity fluctuations (see above) can be violated, and a 'large-scale' mode can be observed in Fig. 4. In addition, weak convective counterflows practically always exist in the cell; they may also lead to slow (with a characteristic time of few seconds) stochastic fluctuations of mean scattering intensity, which will be interpreted by DynaLS as the presence of millimetre-sized particles in the system.

The fact that the size distribution is reproduced at different scattering angles (Fig. 4) suggests that there are particles of submicron and micrometer sizes in the bulk of aqueous salt solution. It is reasonable to suggest that the particles with low optical density, observed in a phase microscope (see Introduction), are nothing more but the micrometre-sized particles found experimentally by DLS (samples of the same NaCl solution were simultaneously studied in both experiments). The main result of the DLS experiment is the fairly wide size distribution of scatterers in the range from several tens of nanometres to several hundreds of nanometres. One can suggest that this wide distribution is due to clusterisation of nanobubbles. Two similar modes, which merge in the range of several hundreds of nanometres (Fig. 4a), are believed to correspond to two different aggregation modes. In our opinion, the small-scale mode corresponds to individual bubstons and clusters, which are formed as a result of bubston self-aggregation (these clusters include only few monomers), while the large-scale mode corresponds to the clusters arising as a result of aggregation on solid impurity centres that were not completely removed by filtering. Therefore, the intensity of this mode should depend on the quality of sample filtering. Indeed, additional filtering reduces the intensity of the large-scale mode, whereas the small-scale mode intensity remains the same. In addition, the large-scale mode turned out to disappear after a very long-term settling (up to six months) of a sample in a hermetic cell, while the small-scale mode remained invariable. Additional experiments must be performed to unambigously determine the internal structure of the particles forming this wide size distribution.

Below we report the results of measuring the correlation functions and corresponding size distributions of scattered light intensity for NaCl solutions with concentrations $C = 0.1$, 10^{-3} и 10^{-5} mol L^{-1} (Figs 5–7). We also measured the correlation scattering functions of solutions in evacuated (to internal pressure of 0.03 atm) ampoules with a physiological solution (sodium chloride with a concentration of 0.165 mol L^{-1}) and in the same ampoules after their unsealing. We could not find any particles in the unsealed (evacuated) ampoule, and the correlation function in the time interval from 10^{-3} to 100 ms coincided with the baseline [see formula (8)]. However, 24 h

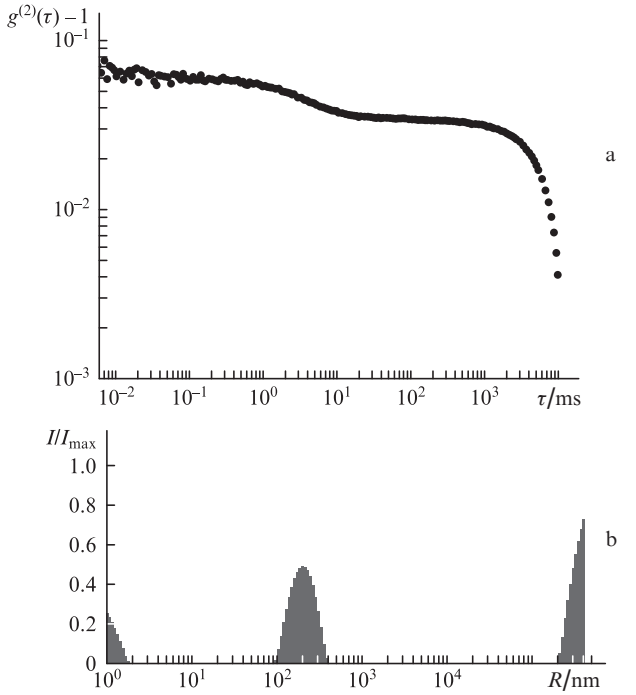

Figure 5. (a) Time correlation function of light intensity scattered at an angle θ = 45° and (b) the corresponding histogram of scattered-light intensity for an aqueous solution of sodium chloride with a concentration of 0.1 mol L^{-1}.

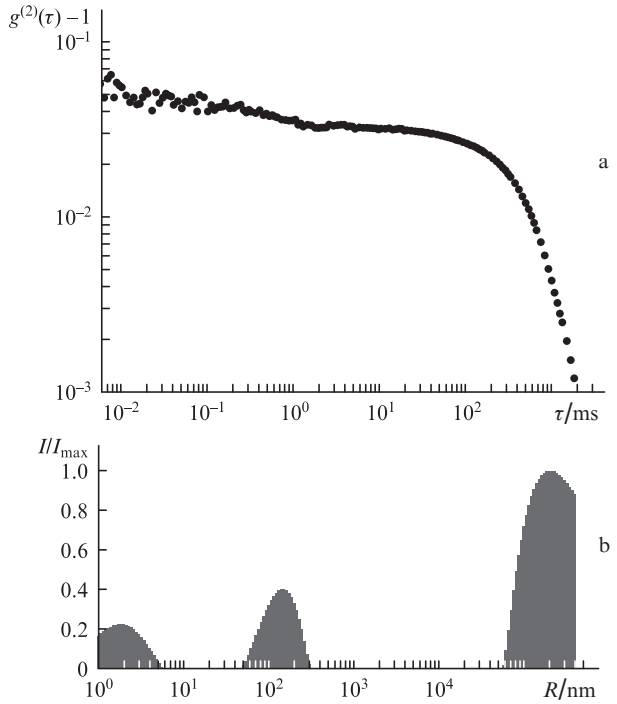

Figure 6. (a) Time correlation function of light intensity scattered at an angle $\theta = 130°$ and (b) the corresponding histogram of scattered-light intensity for an aqueous solution of sodium chloride with a concentration of 10^{-3} mol L^{-1}.

after unsealing (the estimated characteristic time corresponded to the diffusion kinetics of liquid sample saturation with dissolved atmospheric air), particles with a scattering-intensity histogram similar to that reported in Fig. 5 could be detected in the ampoule. Indeed, on the assumption that the diffusion coefficient of molecular gas (for example, nitrogen) in water is $D \sim 10^{-5}$ cm^2 s^{-1} [30] and the characteristic cell depth is 1 cm, we can estimate the time of liquid saturation with dissolved gas as $t \approx 28$ h. We believe that saturation of sample with dissolved air is accompanied by the formation of babston-cluster phase.

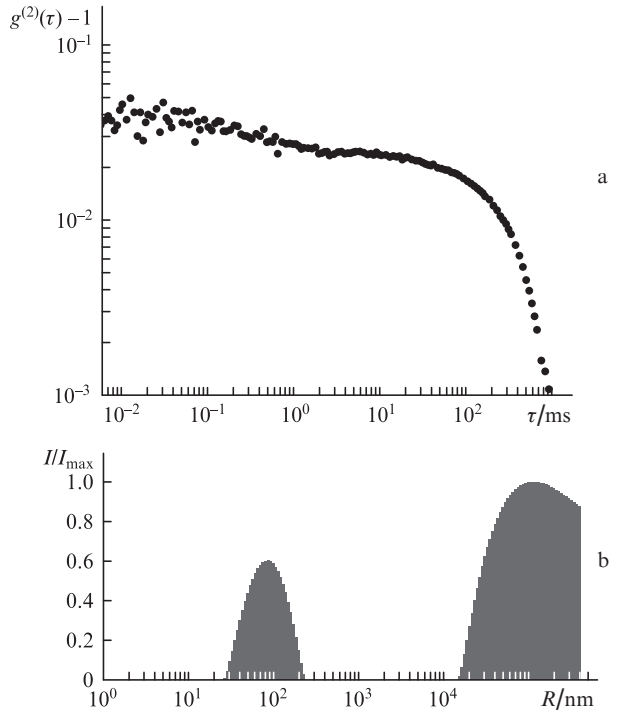

Figure 7. (a) Time correlation function of light intensity scattered at an angle $\theta = 130°$ and (b) the corresponding histogram of scattered-light intensity for an aqueous solution of sodium chloride with a concentration of 10^{-5} mol L^{-1}.

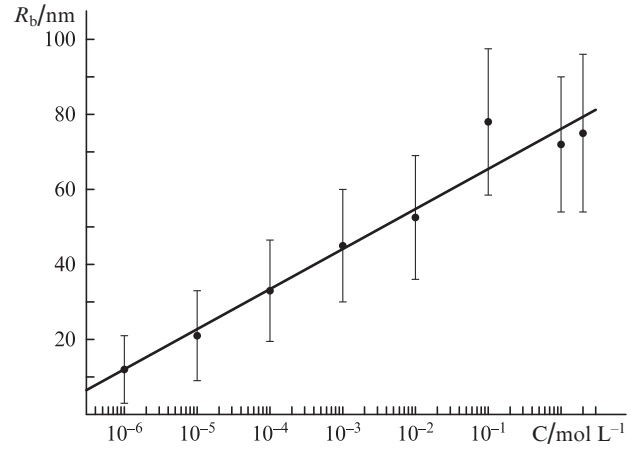

Figure 8. Dependence of the bubston radius (lower boundary of the nanoscale component) on the NaCl concentration: (circles) experimental data and (straight line) a logarithmic approximation.

As was noted above, the behaviour of the obtained histograms of scattering-intensity size distributions depends strongly on the quality of sample filtering and the sample settling time in hermetic cells. At the same time, the lower boundary of the nanoscale component in these histograms varied to a much smaller extent with a change in the aforementioned experimental conditions for all salt concentrations (Figs 5b, 6b, 7b). This behaviour of the histogram of DLS intensity distribution for (10–100)-nm scatterers confirms that these scatterers are bubston clusters containing different numbers of bubstons. In this case, the relatively stable lower boundary of this component corresponds to the bubston size at a specified ion concentration. A dependence of the bubston radius R_b (estimated as the mean position of the lower boundary of the nanoscale component) on the ion concentration C is shown in Fig. 8. Note that in the range $10^{-6} < C < 10^{-2}$ mol L^{-1} the experimental dependence is in good agreement with the predictions of the theory developed in [3].

3. Conclusions

DLS experiments with aqueous NaCl solutions revealed particles characterised by a wide size distribution in a range of 10–1000 nm, the parameters of which depend on the dissolved-salt concentration. Note that no scatterers were found in the cell with a sodium chloride solution evacuated to pressure of 0.03 atm; however, they arose several hours after unsealing the cell.

The particles observed can be interpreted as clusters (containing different numbers of bubstons) and single bubstons. The bubston radius R_b increases with an increase in the dissolved-salt concentration, reaching a value of ~100 nm in concentrated solutions ($10^{-1} < C < 1$ mol L^{-1}).

Acknowledgements. This work was supported by the Russian Foundation for Basic Research (Grant No. 13-02-00731) and 'Origin of Life and Formation of Biosphere' Programme No. 28 of the Presidium of the Russian Academy of Sciences (Subprogramme I 'Physics, Chemistry, and Biology of Water').

References

1. Sirotyuk M.G., in *Moshchnye ul'trazvukovye polya* (High-Power Ultrasonic Fields) (Moscow: Nauka, 1968).
2. Bunkin N.F., Bunkin F.V. *Zh. Eksp. Teor. Fiz.*, **101**, 512 (1992).
3. Bunkin N.F., Bunkin F.V. *Phys. Wave Phenom.*, **21** (2), 81 (2013).
4. Bunkin N.F., Bunkin F.V. *Laser Phys.*, **3**, 63 (1993).
5. Bunkin N.F., Lobeev A.V. *Kvantovaya Elektron*., **21**, 319 (1994) [*Quantum Electron*., **24**, 297 (1994)].
6. Bunkin N.F., Suyazov N.V., Shkirin A.V., Ignatiev P.S., Indukaev K.V. *J. Chem. Phys.*, **130**, 134308 (2009).
7. Bunkin N.F., Ninham B.W., Ignatiev P.S., Kozlov V.A., Shkirin A.V., Starosvetskij A.V. *J. Biophotonics*, **4** (3), 150 (2011).
8. Bunkin N.F., Shkirin A.V., Ignatiev P.S., et al. *J. Chem. Phys.*, **137** (5), 054706 (2012).
9. Bunkin N.F., Shkirin A.V., Suyazov N.V., Starosvetskij A.V. *J. Quant. Spectrosc. Radiat. Transfer*, **123**, Special Issue, 23 (2013).
10. Jungwirth P., Tobias D.J. *Chem. Rev.*, **106**, 1259 (2006).
11. Berne B.J., Pecora R. *Dynamic Light Scattering* (Malabar, Florida: Krieger, 1990).
12. Skazka V.S. *Usp. Khim*., **53** (5), 880 (1985).
13. Einstein A., Smoluchowski M. *Braunovskoe dvizhenie* (Brownian Motion). Ed. by B.I. Davydov (Leningrad: ONTI, 1936).
14. Landau L.D., Lifshitz E.M. *Course of Theoretical Physics, Vol. 5: Statistical Physics* (Oxford: Pergamon, 1980).
15. Dhont J.K.G. *An Introduction to the Dynamics of Colloids* (Amsterdam: Elsevier, 1996).
16. Akhmanov S.A., D'yakov Yu.E., Chirkin A.S. *Vvedenie v statisticheskuyu radiofiziku i optiku* (Introduction to Statistical Radiophysics and Optics) (Moscow: Nauka, 1981).
17. Cummins H.S., Pike E.R. (Eds) *Photon Correlation and Light Beating Spectroscopy* (New York: Plenum, 1974).
18. Yoshimura T. *J. Opt. Soc. Am. A*, **3**, 1032 (1986).
19. Protopopov V.V., Ustinov N.D. *Lazernoe geterodinirovanie* (Laser Heterodyning) (Moscow: Nauka, 1985).
20. Landau L.D., Lifshitz E.M. *Course of Theoretical Physics, Vol. 6: Hydrodynamics* (Oxford: Pergamon, 1984).
21. Tikhonov A.N., Samarskii A.A. *Metody matematicheskoi fiziki* (Methods of Mathematical Physics) (Moscow: Nauka, 1977).
22. Provencher S. *Comput. Phys. Commun.*, **27**, 213 (1982).
23. Provencher S. *Comput. Phys. Commun.*, **27**, 229 (1982).
24. Clementi L.A., Vega J.R., Gugliotta L.M. *Part. Part. Syst. Char.*, **27** (5-6), 146 (2012).
25. http://www.photocor.com/download/dynals/dynals-white-paper.htm.
26. Kovalenko K.V., Krivokhizha S.V., Masalov A.V., Chaikov L.L. *Kr. Soobshch. Fiz. FIAN*, **36** (4), 3 (2009).
27. Van de Hulst H.C. *Light Scattering by Small Particles* (New York: Dover Publications, 1981).
28. Ishimaru A. *Wave Propagation and Scattering in Random Media* (San Diego, California: Academic Press, 1978) Vol. 1.
29. Fabelinskii I.L. *Molekulyarnoe rasseyanie sveta* (Molecular Scattering of Light) (Moscow: Nauka, 1965).
30. Novoselov A.G., Tishin V.B., Duzhii A.B., in *Novyi spravochnik khimika i tekhnologa. Protsessy i apparaty khimicheskikh tekhnologii* (New Handbook of Chemist and Technologist: Processes and Equipment for Chemical Technologies) (St. Petersburg: NPO Professional, 2006) Pt II.